THE JOURNAL OF PHYSICAL CHEMISTRY B



Article

# Phase Behaviors and Structures of a Symmetrically Tapered Biphenylamide

Seok-Ho Hwang, Soo-Jin Park, Hak Yong Kim, Shiao-Wei Kuo, Seung Hee Lee, Myong-Hoon Lee, and Kwang-Un Jeong

*J. Phys. Chem. B*, **2009**, 113 (17), 5843-5854• DOI: 10.1021/jp900666c • Publication Date (Web): 01 April 2009



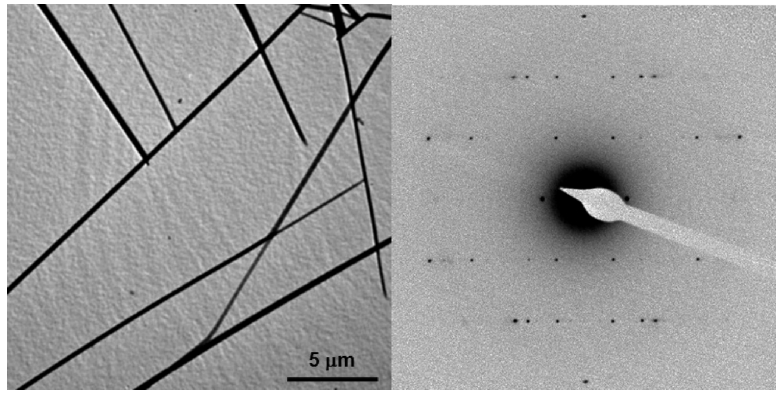


## More About This Article

Additional resources and features associated with this article are available within the HTML version:

- Supporting Information
- Access to high resolution figures
- Links to articles and content related to this article
- Copyright permission to reproduce figures and/or text from this article

View the Full Text HTML



The Journal of Physical Chemistry B is published by the American Chemical Society. 1155 Sixteenth Street N.W., Washington, DC 20036

# Phase Behaviors and Structures of a Symmetrically Tapered Biphenylamide

**Seok-Ho Hwang,[‡,⊥] Soo-Jin Park,[§,⊥] Hak Yong Kim,[§] Shiao-Wei Kuo,[∥] Seung Hee Lee,[†] Myong-Hoon Lee,[†] and Kwang-Un Jeong*[,†]**

*Polymer Materials Fusion Research Center and Department of Polymer-Nano Science and Technology, Chonbuk National University, Jeonju 561-756, Korea; Chonan R&D Center, Korea Institute of Industrial Technology, Chonan 330-825, Korea; Department of Textile Engineering, Chonbuk National University, Jeonju 561-756, Korea; and Department of Materials Science and Optoelectronic Engineering, National Sun Yat-Sen University, Kaohsiung 804, Taiwan*

*Received: January 22, 2009; Revised Manuscript Received: February 27, 2009*

A symmetrically tapered *N*,*N*′-bis[tris[(2-dodecylaminocarbonyl)ethyl]methyl]]-4,4′-biphenylamide (d-C$_n$PhA, where $n$ is the number of carbon atoms in the alkyl chains, $n = 12$), was newly designed and synthesized in order to investigate the supramolecular ordered structures induced by phase separation, hydrogen (H)-bonding, and $\pi-\pi$ stacking interaction. This symmetrically tapered d-C$_{12}$PhA biphenylamide consists of three different parts: H-bondable hydrophilic amide moieties, a rigid hydrophobic biphenyl aromatic core, and three flexible hydrophobic alkyl chains at each end of the core. Major phase transitions and supramolecular structures in d-C$_{12}$PhA biphenylamide were characterized by differential scanning calorimetry (DSC), one-dimensional (1D) wide-angle X-ray diffraction (WAXD), 1D and 2D Fourier-transform infrared spectroscopy (FT-IR), and solid-state $^{13}$C nuclear magnetic resonance (NMR). The symmetrically tapered d-C$_{12}$PhA biphenylamide formed a hexagonal columnar ($\Phi_H$) liquid crystalline (LC) mesophase at a cooling process and a highly ordered columnar ($\Phi_{HK}$) crystalline phase at a subsequent heating process. Selected area electron diffractions (SAED) from single crystals combined with the results of WAXD and POM suggest that discotic building blocks are constructed by three d-C$_{12}$PhA biphenylamides rotating 60° with respect to neighboring ones and the ABC stacked discotic building blocks further self-assemble into columns and then these columns are laterally close-packed to give nanorods. Furthermore, it was identified that the long axis of column is parallel to the long axis of rods.

## Introduction

Since the first discovery of liquid crystalline (LC) materials in the 1880s, the relationships between the formation of LC mesophases and the structures of the constituent molecules have been major research topics.[1−3] When the thermotropic LC of rodlike molecules (calamitic LC) started to revolutionize commercial LC display technologies, Chandrasekhar et al. first reported the formation of LC phase from a disclike molecule (discotic LC) in 1977.[1] Exponentially accelerated development of LC display (LCD) technology utilizing calamitic LCs makes LCDs an essential part of our everyday life and it looks like that discotic LCs cannot compete with calamitic LCs in terms of electro-optical displays.[1−3] However, due to the many extraordinary properties of discotic LCs such as one-dimensional (1D) electrical conductivity,[4] fast photoconductivity,[5] and ferroelectricity,[6] the structures and dynamics of discotic LCs have been studied extensively for practical applications and scientific challenges.[1] In addition to the traditional discotic LCs consisting of discogenic molecules as building blocks which possess a disclike rigid core with flexible tails, many novel discotic LCs have been introduced, including those with building blocks that are chiral molecules, inverted molecules, tapered molecules, half-disc molecules, dendrimers, or symmetric-tapered molecules.[7]

The formation of columnar phases has been traditionally through a process of self-organization of discotic supermolecules, giant molecules made of covalently bonded smaller identifiable components.[1] Recently, a process of self-assembly through noncovalent interactions provides a new approach to design and synthesis of programmed functional soft materials. Noncovalent interactions include hydrogen bonding, electrostatic (ion−ion, ion−dipole, and dipole−dipole), $\pi-\pi$ stacking, van der Waals interactions, and hydrophobic−hydrophilic effects along with others.[8] The hydrophobic−hydrophilic phase separation between two incompatible yet chemically bonded components often used in block copolymers has been successfully applied as a driving force to facilitate the formation of self-assembled columnar structures.[2,3,8] This can happen between rigid aromatic discotic cores and flexible alkyl parts. Since the rigid aromatic discotic cores and flexible alkyl parts are covalently bonded, only nanoscopic phase separation is allowed. Depending on the volume fractions of each component, various nanostructures have been constructed from smectic phases, laminated phases, to polygonal columnar phases.[1−3] In addition to the phase separation, H-bonding has become one of the major tools to program building blocks of supramolecular structures due to its moderate bonding energy, directionality, selectivity and reversibility.[2,3] In these H-bonding systems, self-assembled columnar structures are not formed by the self-organization of discotic supermolecules but constructed by the self-assembly

* To whom correspondence should be addressed. E-mail: kujeong@chonbuk.ac.kr.
† Polymer Materials Fusion Research Center and Department of Polymer-Nano Science and Technology, Chonbuk National University.
‡ Korea Institute of Industrial Technology.
§ Department of Textile Engineering, Chonbuk National University.
∥ National Sun Yat-Sen University.
⊥ These authors contributed equally to this work.

10.1021/jp900666c CCC: $40.75 
Published on Web 04/01/2009

of supramolecular discs as building blocks generated through intra/intermolecular H-bonding.

Recently, self-assembled discotic building blocks were constructed by combining both H-bonding and phase separation processes in symmetric-tapered bisamides (CnPhBA).[9] It was found that a self-assembled disc was generated through intermolecular H-bonding and phase separation of the rigid cores and alkyl tails, and these supramolecular discs further self-organized into oblique columnar phases. The question remains: what is the molecular packing when the spatial steric hindrance is involved and the H-bondable amine functions are located between an aromatic core and flexible alkyl tails?

In order to find possible answers to this question and to investigate the supramolecular ordered structures induced by phase separation, $\pi-\pi$ stacking interactions and H-bonding, a symmetrically tapered *N*,*N*′-bis[tris[(2-dodecylaminocarbonyl)-ethyl]methyl]]-4,4′-biphenylamide (d-C$_n$PhA, $n = 12$) was newly designed and synthesized. Differential scanning calorimetry (DSC) was utilized to detect the thermal transitions in this d-C$_{12}$PhA sample. The phase structures of d-C$_{12}$PhA were identified by wide-angle X-ray diffraction (WAXD) at different temperatures and selected area electron diffraction (SAED) from single crystals. The phase morphologies in the ordered phases were further investigated via polarized optical microscopy (POM). The H-bonding between N−H and C═O groups were studied using Fourier-transform infrared spectroscopy (FT-IR). The dynamic conformational changes of the aromatic and aliphatic parts of d-C$_{12}$PhA at different temperatures correspond well with the thermal transitions via solid-state carbon−13 nuclear magnetic resonance ($^{13}$C NMR) experiments. The d-C$_{12}$PhA forms two ordered phases below the isotropic temperature. The hexagonal columnar ($\Phi_H$) mesophase is constructed during a cooling process and this $\Phi_H$ phase transforms a highly ordered hexagonal columnar ($\Phi_{HK}$) crystalline phase during a subsequent heating process. On the basis of our experimental observations, we conclude that the discotic building block is constructed by three d-C$_{12}$PhA biphenylamides rotating 60° with respect to neighboring ones and the ABC stacked discotic building blocks further self-assemble to columns which are laterally close-packed to hexagonal columnar phases. Furthermore, d-C$_{12}$PhA forms nanorods via the molecular self-assembly and self-organization process.

## Experimental Section

**Materials and Sample Preparation.** A symmetrically tapered *N*,*N*′-bis[tris[(2-dodecylaminocarbonyl)ethyl]methyl]]-4,4′-biphenylamide (d-C$_{12}$PhA, where *n* is the number of carbon atoms in the alkyl chains, $n = 12$) was newly synthesized via simple peptide coupling reactions.[10] The detailed synthetic procedures for d-C$_{12}$PhA are shown in Scheme 1. The final compound was purified through repeated chromatography with a silica gel using an acetone−benzene (5:95) mixture as the eluting solvent, followed by recrystallization from an ethanol−benzene mixture and vacuum drying. The purity of the materials was verified by thin layer chromatography (TLC) and proton nuclear magnetic resonance ($^1$H NMR). Chemical structure of d-C$_{12}$PhA was confirmed by $^1$H NMR spectroscopy in $CDCl_3$ solution: $\delta$ 8.10 (s, −CON*H*−, 4H), 7.99 (d, 2,6-Ar*H*, 2,6-Ar′*H* 4H), 7.66 (d, 3,5-Ar*H*, 3,5-Ar′*H*, 4H), 3.22 (m, −CONHC$H_2$−, 12H), 2.18 (m, −C(CH$_2$C$H_2$−)$_3$, 12H), 1.91 (m, −C(C$H_2$CH$_2$−)$_3$, 12H), 1.25 (m, −CONHCH$_2$(C$H_2$)$_{10}$CH$_3$, 40H), and 0.86 (m, −CONHCH$_2$(CH$_2$)$_{10}$C$H_3$, 18H).

For one-dimensional (1D) wide-angle X-ray diffraction (WAXD) measurements, film samples with a thickness of about 1 mm were prepared by melting the compounds on an aluminum plate. The samples prepared for POM had a typical thickness of 10 $\mu$m, and they were melt-processed between two bare cover glass sides. The film samples for Fourier transform infrared spectroscopy (FT-IR) were prepared by film casting from a $CHCl_3$ dilute solution onto KBr plates and the solvent was evaporated. The powder samples were used for solid-state carbon-13 ($^{13}$C) nuclear magnetic resonance (NMR). Thin film samples prepared for transmission electron microscopy (TEM) via solution casting from a 0.05% (w/v) chloroform solution onto carbon-coated mica had a thickness of 50−150 nm. After crystallization and annealing process, the films were floated onto the water surface and recovered using the TEM copper grids.

**SCHEME 1**

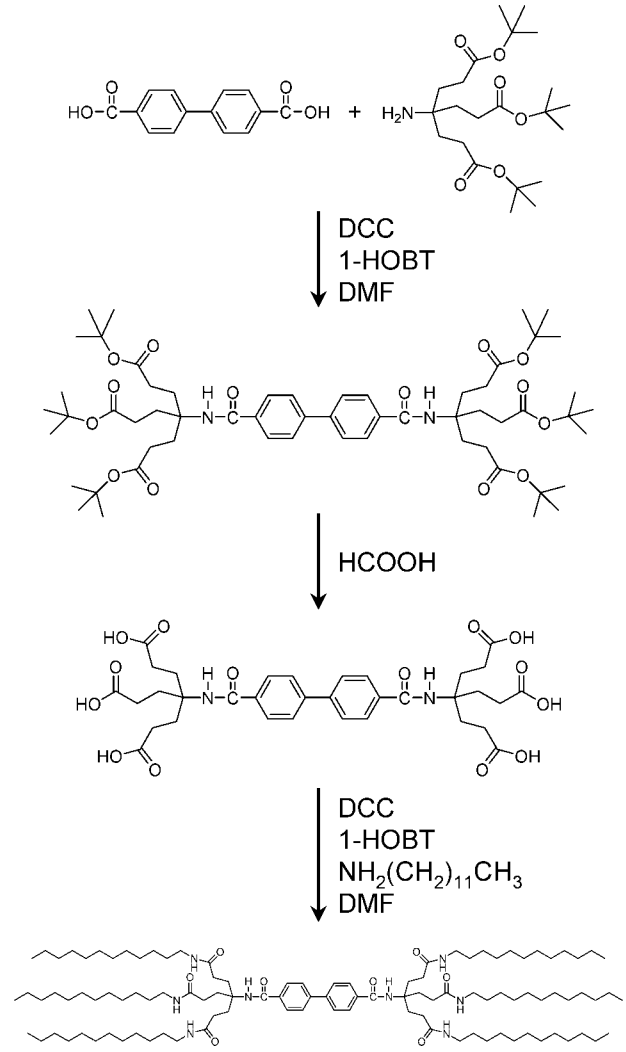


**Equipment and Experiments.** The thermal behavior of the phase transitions was studied using a Perkin-Elmer PYRIS Diamond DSC with an Intracooler 2P apparatus. The temperatures and heat flows were calibrated using standard materials at cooling and heating rates ranging from 2.5 to 40 °C/min. The heating experiments always preceded the cooling experiments in order to eliminate previous thermal histories, and the cooling and heating rates were always kept identical. The transition temperatures were determined by measuring the onset and/or peak temperatures from both the cooling and heating scans at different rates.

1D WAXD powder experiments were conducted in the reflection mode of a Rigaku 12 kW rotating-anode X-ray (Cu

Kα radiation) generator coupled to a diffractometer. The diffraction peak positions and widths were calibrated with silicon crystals in the high $2\theta$ angle region (>15°) and silver behenate in the low $2\theta$ angle region. A hot stage was coupled to the diffractometer in order to study the structural evolutions with temperature changes during heating and cooling. The temperature of this hot stage was calibrated to be within ±1 °C. Samples were scanned across a $2\theta$ angle range of 1.5° to 35° at a scanning rate of 4 deg/min. The background scattering was subtracted from the sample scans.

Bright images of TEM (FEI Tacnai 12) were obtained to examine crystal morphology on the nanometer scale using an accelerating voltage of 120 kV. The camera length was set at 3 m and calibration of the SAED spacing smaller than 0.384 nm was carried out using evaporated thallous chloride, which has the largest first-order spacing diffraction of 0.384 nm. Spacing values larger than 0.384 nm were calibrated by doubling the *d*-spacing values of the first-order diffractions.

Optical textures of the ordered phases at different temperatures were observed with a POM (Olympus BH-2) coupled with a Mettler heating stage (FP-90) in order to investigate morphology on the micrometer scale. A tint retardation plate (530 nm) was also placed between the objective lenses and the eyepieces in order to identify the orientation of molecules in the POM textures. H-bonding and molecular chain conformations were studied using a FT-IR (Digilab Win-IR Pro FTS 3000) equipped with a Bruker heating stage. The resolution was 1 $cm^{-1}$ and 40 scans were averaged for each spectrum. The temperatures of this hot stage were calibrated to be within ±0.5 °C. The dynamics of each carbon and the conformations of the alkoxyl chain in d-$C_{12}$PhA at different temperatures were also studied using a solid-state $^{13}C$ NMR (Chemagnetics CMX 200) operating at 201.13 and 50.78 MHz for $^{1}H$ and $^{13}C$ nuclei. The samples were spun in nitrogen gas at 4.5 kHz at the magic angle. The magic angle was optimized by the intensity calibration of the aromatic carbon resonance of hexamethylbenzene. The $^{13}C$ cross-polarization/magic angle spinning/dipolar decoupling (CP/MAS/DD) NMR spectra were acquired to selectively investigate the rigid components and the Bloch decay spectra with MAS/DD was used to selectively study the mobile components. The CP contact time was 1 ms, while the recycle time of the pulse was 5 s. Each spectrum consisted of an accumulation of 500 scans. The temperature of the solid-state $^{13}C$ NMR experiment was controlled using a REX-F900 VT unit covering the temperature range from −70 to 210 °C.

Overlapped C═O and N−H absorption peaks in FT-IR, characteristic carbon peaks in solid-state $^{13}C$ NMR, and thermal transitions in DSC were resolved using the PeakFit peak separation program (Jandel Scientific). Symmetric/asymmetric Gaussian and Lorentzian functions were used to obtain the best fit, respectively. The Cerius$^2$ (Version 4.6) simulation software from Accelrys was used to calculate the minimal energy geometry of the symmetrically tapered d-$C_{12}$PhA compound in the isolated gas phase utilizing the COMPASS force field.

## Results and Discussion

**Geometric Dimension and Shape of d-$C_{12}$PhA.** As represented in Figure 1a,b, the symmetrically tapered d-$C_{12}$PhA consists of three different parts: H-bonded hydrophilic amide moieties, a rigid hydrophobic biphenyl core, and three flexible hydrophobic alkyl chains at each end of the core. Because of H-bondable hydrophilic amide moieties between rigid hydrophobic aromatic core and flexible hydrophobic alkyl chains, hydrophilic−hydrophobic phase separation could be enhanced

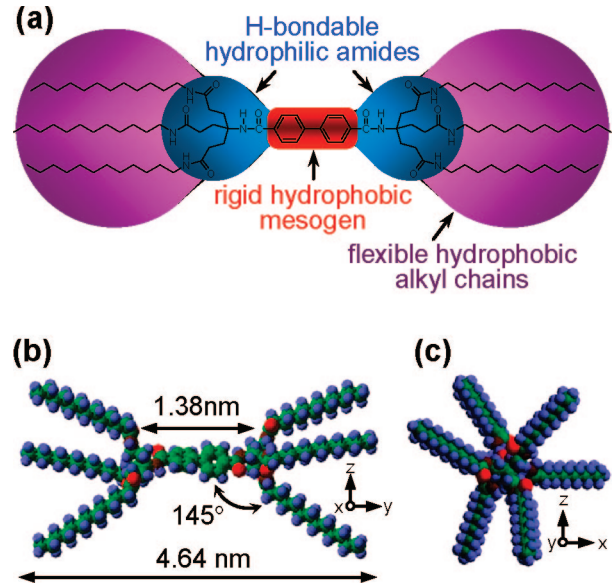


**Figure 1.** Schematic illustration of d-$C_{12}$PhA compound (a). Computed energy-minimized spacing dimensions and shapes of d-$C_{12}$PhA with side (a) and head (b) views.

during self-assembly and self-organization processes. Furthermore, relatively smaller volume of rigid aromatic core compared with hydrophobic alkyl chains at each side of the rigid core can induce steric hindrances which could be one of the dominant factors to determine the close-packing assembly. The whole shape of d-$C_{12}$PhA looks like a dumbbell, as illustrated in Figure 1a. In order to know the precise 3D geometric dimensions and shape of d-$C_{12}$PhA, computer calculation of the conformational minimum free energy of d-$C_{12}$PhA in the isolated vacuum state was carried out using Cerius$^2$ 4.6 software. The energy-minimized side and head views of d-$C_{12}$PhA are shown in Figure 1b and 1c, respectively. The global equilibrium geometry of d-$C_{12}$PhA was constructed at 0 K using the COMPASS force field. As shown in Figure 1b, biphenyl aromatic core and amide functions right at the end of the rigid aromatic core are on the same line, and its length is 1.38 nm. Hydrophobic alkyl chains at each side of the rigid core are in the zigzag conformation and they made 145° angles with respect to the aromatic core. Therefore, three alkyl chains at each side of the rigid core made 3D corn shapes, which may induce a steric hindrance during the self-assembly process. The total length of d-$C_{12}$PhA is 4.64 nm, which is smaller than that of the fully extended length.

**Thermal Properties of Phase Transformations.** Figure 2a shows sets of DSC cooling and subsequent heating thermal diagrams at different cooling and heating rates in the range of 2.5 to 40 °C/min. First of all, thermal transition behaviors strongly depend on the cooling and heating rates. At 10 °C/min cooling rate, d-$C_{12}$PhA does not show any obvious thermal transitions during cooling process. However, a subsequent heating at 10 °C/min exhibits a sudden step change of heat capacity around 50 °C which belongs to the glass transition temperature ($T_g$). At 83 °C, which is 33 °C above $T_g$, an exothermic thermal transition with −11.5 J/g (−19.6 kJ/mol) enthalpy change was observed. This exothermic thermal transition could be a recrystallization and/or reorganization of d-$C_{12}$PhA. When the temperature reached 130 °C, a broad endothermic thermal transition started and overlapped with another endothermic thermal transition having the peak temperature at 153 °C. The total enthalpy change of these two thermal transitions was measured to 23.1 J/g (39.4 kJ/mol). In order to confirm the existence of two thermal transitions as well

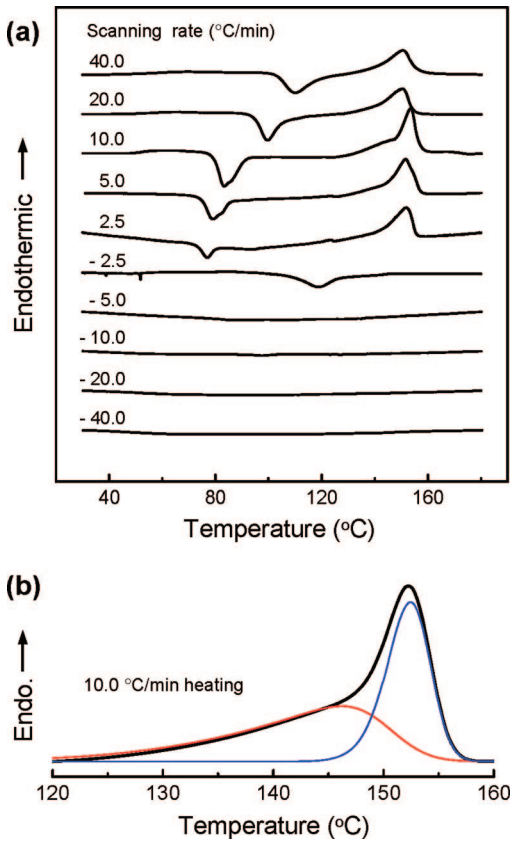


**Figure 2.** Sets of DSC cooling and subsequent heating thermal diagrams for d-$C_{12}$PhA at scanning rates ranging from 2.5 to 40 °C/min (a). Analytical deconvolution of a DSC thermal diagram at a heating rate of 10 °C/min.

as to know the amount of heat change during the transitions, the DSC thermal diagram was resolved using the PeakFit peak separation program. Asymmetric Gaussian functions were used to obtain the best fit. As represented in Figure 2b, the overlapped DSC thermal transitions were deconvoluted to two thermal transitions with peak temperatures at 145 °C (12.2 J/g, 53%) and 153 °C (10.9 J/g, 47%), respectively. The amount of heat changes at two thermal transitions depend on the cooling and heating rates so that this thermal transition should be related with kinetics of reorganization of d-$C_{12}$PhA. The faster heating rate, the more heat change at 145 °C. Above 20 °C/min heating rate, the thermal transition at 153 °C is almost depressed, which could be due to the less period of time for d-$C_{12}$PhA to be reorganized.

**Molecular Origins of the Phase Transformations.** Although DSC experiments are sensitive to heat absorption and release events during thermal transition and can give quantitative thermodynamic values, this technique does not usually provide direct information of the molecular origins of structural changes. Therefore, FT-IR and solid-state $^{13}C$ NMR experiments at different temperatures in the range of 30−170 °C were combined with DSC results to identify the possible molecular origins of structural evolutions. Figure 3a shows the FT-IR spectrum of d-$C_{12}$PhA sample at 30 °C, which is prepared by cooling at 2.5 °C/min from the isotropization temperature ($T_i$ = 153 °C). The characteristic bands of aromatic biphenyl rings appear at 1610, 1582, 1527, and 1493 $cm^{-1}$.[11] The N−H stretching vibration of amide groups exhibits a broad absorption band with the maximum intensity at 3300 $cm^{-1}$, and the amide I, II, and III motions generate absorption bands at 1642, 1547, and 1232 $cm^{-1}$, respectively.[11] The absorption bands attributed to the alkyl chains can be found at 2956 $cm^{-1}$ (asymmetric stretching band of $CH_3$), 2924 $cm^{-1}$ (asymmetric stretching band of $CH_2$), 2873 $cm^{-1}$ (symmetric stretching of $CH_3$), and 2853 $cm^{-1}$ (symmetric stretching of $CH_2$), respectively.[11]

With careful examinations of frequency, intensity, and shape of absorption bands at different temperatures, conformational and molecular interactions of d-$C_{12}$PhA in phases and during phase transitions can be investigated. Extensive H-bonding between the N−H group of one amide unit and the C═O of another in d-$C_{12}$PhA can impose prominent influence on the involved IR bands. The H-bonding sensitive N−H stretching vibration band (3293 $cm^{-1}$) and amide I mode (1642 $cm^{-1}$) mainly from the carbonyl stretching vibration clearly indicate that at room temperature almost all the N−H groups in d-$C_{12}$PhA are associated with the C═O groups via N−H···O═C H-bonds (Figure 3a). The amide I mode which is sensitive to H-bonds as well as to local conformational changes shows a broad absorption band between 1600 and 1700 $cm^{-1}$, which can be resolved to three spectral contributions.[11] A narrow band between 1635 and 1642 $cm^{-1}$ with a width at half-height of 20 $cm^{-1}$ stands for the H-bonded C═O groups in ordered domains, while a broad band between 1645 and 1654 $cm^{-1}$ with a width at half-height of 40 $cm^{-1}$ is originated from the H-bonded C═O groups in disordered domains. Finally, an absorption band between 1678 and 1683 with a width at half-height of 25 $cm^{-1}$ is due to the free C═O groups. The N−H stretching mode between 3200 and 3500 $cm^{-1}$ consists of two different spectral contributions. A weak and relatively narrow band at 3448 $cm^{-1}$ is for the free N−H groups, while a broad band between 3200 and 3400 $cm^{-1}$ is assigned to H-bonded N−H groups.

On cooling from 180 to 140 °C at 2.5 °C/min, the intensity and area of free N−H bands is decreased by increasing the intensity of H-bonded N−H band with the gradual shift of maximum intensity from 3335 to 3312 $cm^{-1}$, as shown in Figure 3b. At the same time in the amide I mode, the amount of free C═O groups is decreased by concomitantly increasing the intensity and area of the band for H-bonded C═O groups in disordered domains. It is worthwhile to note that significant dissociation of H-bonds only takes place above the isotropization temperature but more than 80% of amide groups participate to form the disordered H-bonds even in the isotropic phase. As shown in Figure 3b, when the temperature reaches the phase transition temperature at 130 °C, the amount of free C═O groups and N−H groups suddenly drops below 5% with a significant increase of the intensity and area of bands for H-bonded N−H and H-bonded C═O groups in ordered domains. This IR result is well matched with that of DSC in Figure 2a. Up to 125 °C during the subsequent heating process at 2.5 °C/min, the intensity of absorption bands for H-bonded N−H and H-bonded C═O groups in ordered domains is gradually decreased, but the bands for free N−H and C═O groups are not emerged at all. This IR result indicates that the exothermic thermal tradition at 77 °C during heating, as shown in Figure 2a, does not involve the significant change of the H-bonds between N−H and C═O. When the temperature is increased up to 135 °C, the onset temperature of the broad endothermic transition, the intensity of absorption bands for H-bonded N−H and H-bonded C═O groups in ordered domains is abruptly dropped with the increases of the intensity of absorption bands of free N−H and C═O groups as well as of H-bonded C═O groups in disordered domains, and the spectra do not change up to 150 °C. This IR result explains the fact that the broad endothermic thermal transition at 145 °C involves a partial dissociation of H-bonding between N−H and C═O groups and certain local conforma-

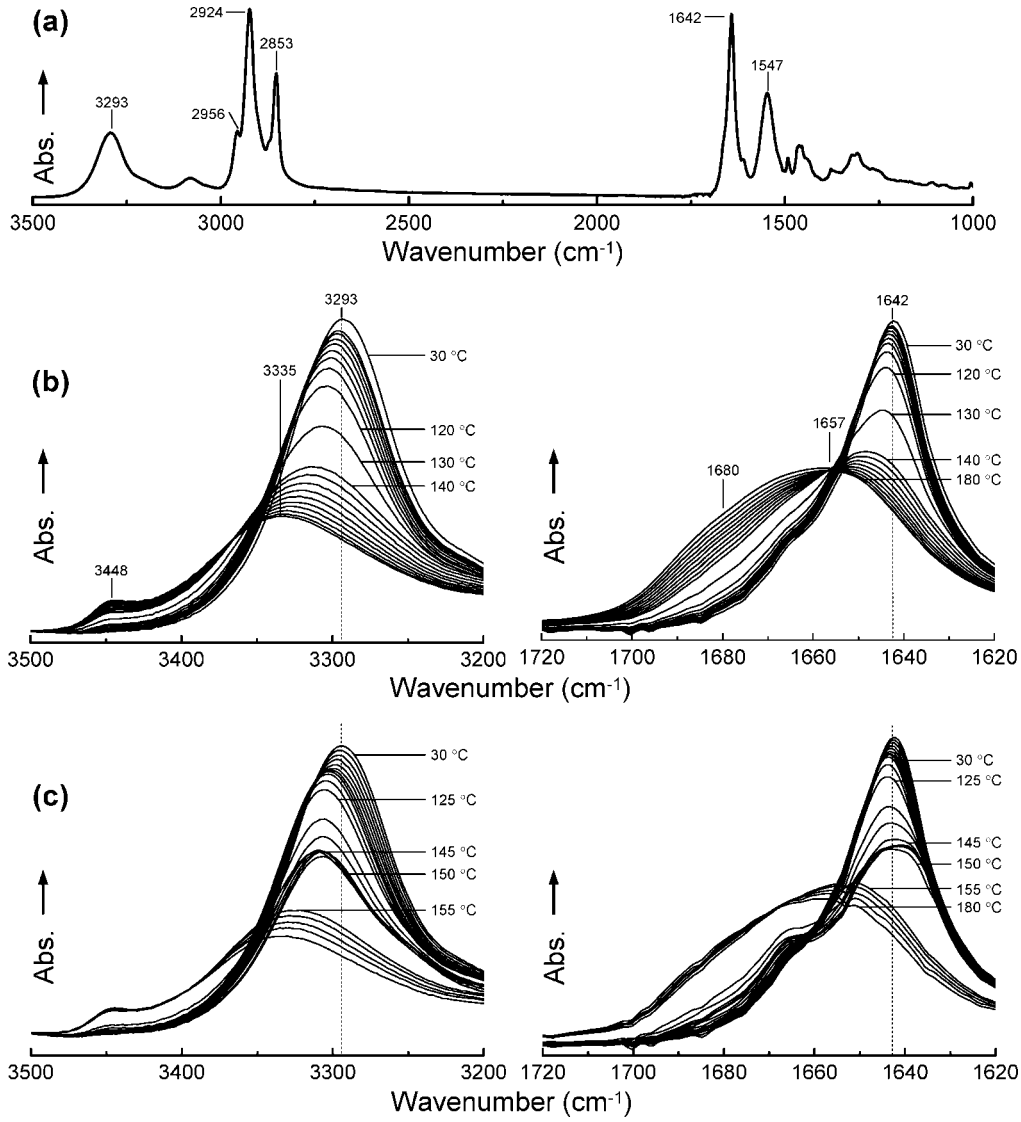


**Figure 3.** FT-IR spectrum of d-$C_{12}$PhA at room temperature after cooling from the isotropic phase at 2.5 °C/min (a). FT-IR spectra of d-$C_{12}$PhA during cooling (b) and subsequent heating (c) at the rate of 2.5 °C/min: 3500−3200 $cm^{-1}$ (N−H) and 1720−1620 $cm^{-1}$ (amide I mode) regions between 180 and 30 °C.

tional changes. Note that there are two types of amide functions in d-$C_{12}$PhA. One is attached at the end of aromatic core and the other is attached in alkyl chains, and the amount of amide functions in d-$C_{12}$PhA is 25% and 75%, respectively. After considering the amount and frequency of amide functions in d-$C_{12}$PhA, it is clear that the broad endothermic thermal transition at 145 °C is accompanied with the dissociation and/or rearrangement of H-bonds in amide functions at the end of aromatic core. Continuous heating up to 155 °C, the temperature above the endothermic thermal transition at 153 °C (Figure 2b), suddenly increases the amount of free N−H and C═O groups of amide functions in alkyl chains.

In order to investigate the phase transition by the environmental changes of functional groups in a molecular dimension, 2D FT-IR correlation spectroscopy is also generalized, as shown in Figure 4a and 4b. 2D FT-IR correlation spectroscopy can identify different intra- and intermolecular interactions through the analysis of selected bands from the 1D vibration spectrum. White and shaded areas in 2D FT-IR correlation contour maps represent positive and negative cross peaks, respectively. 2D FT-IR correlation spectra are characterized by two independent wavenumber axes and a correlation intensity axis.[11] In general, two types of spectra, 2D synchronous and asynchronous, are obtained; the correlation intensities in the 2D synchronous and asynchronous maps reflect the relative degrees of in-phase and out-of-phase responses, respectively. The 2D synchronous spectra are symmetric with respect to the diagonal line in the correlation map. Auto peaks, which represent the degree of autocorrelation of perturbation-induced molecular vibrations, are located at the diagonal positions of a synchronous 2D spectrum; their values are always positive. When an auto peak appears, the signal at that wavenumber would change greatly under environmental perturbation. Cross peaks located at off-diagonal positions of a synchronous 2D spectrum (they may be positive or negative) represent the simultaneous or coincidental changes of the spectral intensity variations measured at $\upsilon_1$ and $\upsilon_2$. Positive cross peaks emerge when the intensity variations of the two peaks at $\upsilon_1$ and $\upsilon_2$ occur in the same direction (i.e., both increase or both decrease) under the environmental perturbation. On the other hand, negative cross peaks reveal that the intensities of the two peaks at $\upsilon_1$ and $\upsilon_2$ change in opposite directions (i.e., one increases while the other decreases) under perturbation.[11] As in the case for a synchronous spectrum, the sign of an asynchronous cross peak can be either negative or positive,

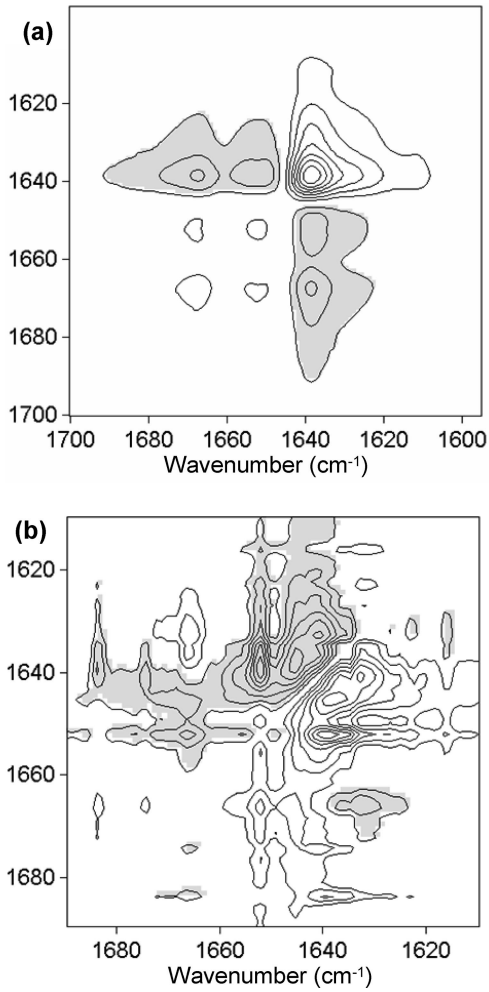


**Figure 4.** Synchronous (a) and asynchronous (b) 2D FT-IR correlation spectra of d-$C_{12}$PhA under temperature perturbation. White and shaded areas in 2D FT-IR correlation contour maps represent positive and negative cross peaks, respectively.

providing useful information on the sequential order of events observed by the spectroscopic technique along the external variable. The 2D asynchronous spectra are asymmetric with respect to the diagonal line in the correlation map. According to Noda's rule,[11] when $\Phi(\upsilon_1,\upsilon_2) > 0$, if $\psi(\upsilon_1,\upsilon_2)$ is positive (black colored area), band $\upsilon_1$ will vary prior to band $\upsilon_2$; if $\psi(\upsilon_1,\upsilon_2)$ is negative (white colored area), band $\upsilon_2$ will vary prior to band $\upsilon_1$. This rule is reversed, however, when $\Phi(\upsilon_1,\upsilon_2) < 0$ In summary, if the symbols of the cross peak in the synchronous and asynchronous maps are the same (both positive or both negative), band $\upsilon_1$ will vary prior to band $\upsilon_2$; if the symbols of the cross peak are different in the synchronous and asynchronous spectra (one positive and the other negative), band $\upsilon_1$ will vary after $\upsilon_2$ under the environmental perturbation.

Figure 4a presents the synchronous 2D correlation maps of d-$C_{12}$PhA sample in the range of 1600−1700 $cm^{-1}$ under the temperature perturbation. Absorption bands in this spectrum have been assigned as mentioned above, 1642 $cm^{-1}$ is corresponding to H-bonded C═O groups in ordered domains, 1657 $cm^{-1}$ is originated from the H-bonded C═O groups in disordered domains, and 1680 is due to the free C═O groups. Clear and positive cross-peaks existed between the signal at 1680 $cm^{-1}$ and 1657 $cm^{-1}$, implying these two functional groups exhibit the same direction with the increase of temperature according to Noda's rule. On the contrary, two negative cross peaks were observed at (1642 vs 1657 $cm^{-1}$) and (1642 vs 1680 $cm^{-1}$), indicating that the band at 1642 $cm^{-1}$ varies in opposite direction with 1657 and 1680 $cm^{-1}$. From these results, it is no doubt to mention that the free carbonyl groups and H-bonded carbonyl groups in disordered domain should vary in opposite direction with the H-bonded order domain.

Figure 4b shows the asynchronous 2D correlation maps in the range of 1610−1700 $cm^{-1}$. The cross peaks among 1680 $cm^{-1}$ with 1657, 1680, and 1642 $cm^{-1}$, and 1657 $cm^{-1}$ with 1642 $cm^{-1}$, show opposite intensity order. It clearly indicates that the peak of 1657 $cm^{-1}$ first alters before that of 1680 $cm^{-1}$ which changes before that of 1642 $cm^{-1}$ during temperature perturbation. This result implies that the H-bonded carbonyl groups in disorder domain first dissociate, then free carbonyl groups and H-bonded carbonyl groups in order domain finally drop with the increase of temperature, which is well matched with the results of DSC.

While the N−H stretching vibration mode and amide I in d-$C_{12}$PhA can be correlated with H-bonding (Figure 3), the asymmetric and symmetric stretching bands of $CH_2$ at 2924 and 2853 $cm^{-1}$, respectively, can be utilized to probe alkyl chain conformations. It is known that, for an all-trans alkyl chain, the asymmetric and symmetric stretching band of $CH_2$ are typically in the ranges of 2846−2850 and 2916−2925 $cm^{-1}$, respectively.[11] However, the changes of the asymmetric and symmetric stretching bands of $CH_2$ in d-$C_{12}$PhA at different temperatures are not so obvious to distinguish the trans−gauche transitions at different phases. Therefore, solid-state $^{13}C$ NMR experiments of d-$C_{12}$PhA at different temperatures with both CP/MAS/DD and Bloch decay methods[12] were conducted to evaluate the ordered (all-trans) and disordered (mixture of trans and gauche) conformational changes of alkyl chains and the mobility of each carbon in d-$C_{12}$PhA in different phases. The CP/MAS/DD method (Figure 5b) is sensitive to the rigid components, and the mobile components can easily be detected by the Bloch decay method (Figure 5c). Chemical shift identifications are carried out by both the solution $^{13}C$ NMR and theoretical calculations based on the tabulated data.[11,12] The chemical shifts at 174 and 168 ppm result from the carbon atoms in the carbonyl groups of amide functions attached at the end of biphenyl core and in the alkyl chains, respectively. The chemical shifts between 100 and 150 ppm come from the carbon atoms in the aromatic biphenyl groups, as shown in Figure 4a and 4b. In addition, the $^{13}C$ chemical shift at 57 ppm represents the carbon atoms at the α position, and the $\beta$ and $\gamma$ carbon atoms appeared at 32 and 24 ppm, respectively. The chemical shifts for other carbons also were identified as shown in Figure 4a,b. The $\beta$ carbon chemical shift in the Bloch decay method (Figure 5c) consists of two values resulting from all-trans sequences (34−32 ppm) and gauche/trans random sequences (32−30 ppm) of the alkyl chains. The intensities of chemical shifts above 100 ppm do not change much during the heating process, but above the isotropization temperature ($T_i$ = 153 °C) they are suddenly increased in solid-state $^{13}C$ NMR spectra with the Bloch decay method (Figure 5c) and decreased in solid-state $^{13}C$ NMR spectra with CP/MAS/DD method (Figure 5b). These solid-sate $^{13}C$ NMR results inform that carbon atoms in carbonyl and aromatic groups are mobile in the isotropic phase, while the solid-sate $^{13}C$ NMR spectra of d-$C_{12}$PhA above 100 ppm are not sensitive to distinguish the mobility of carbons in different ordered phases. The $\beta$ chemical shift at 33 ppm corresponding to the methylene carbon atoms in the ordered segments of alkyl tails increases from 25 to 45% as the temperature is raised from 30 to 100 °C, while the chemical shift peak at 31 ppm representing the methylene carbon atoms

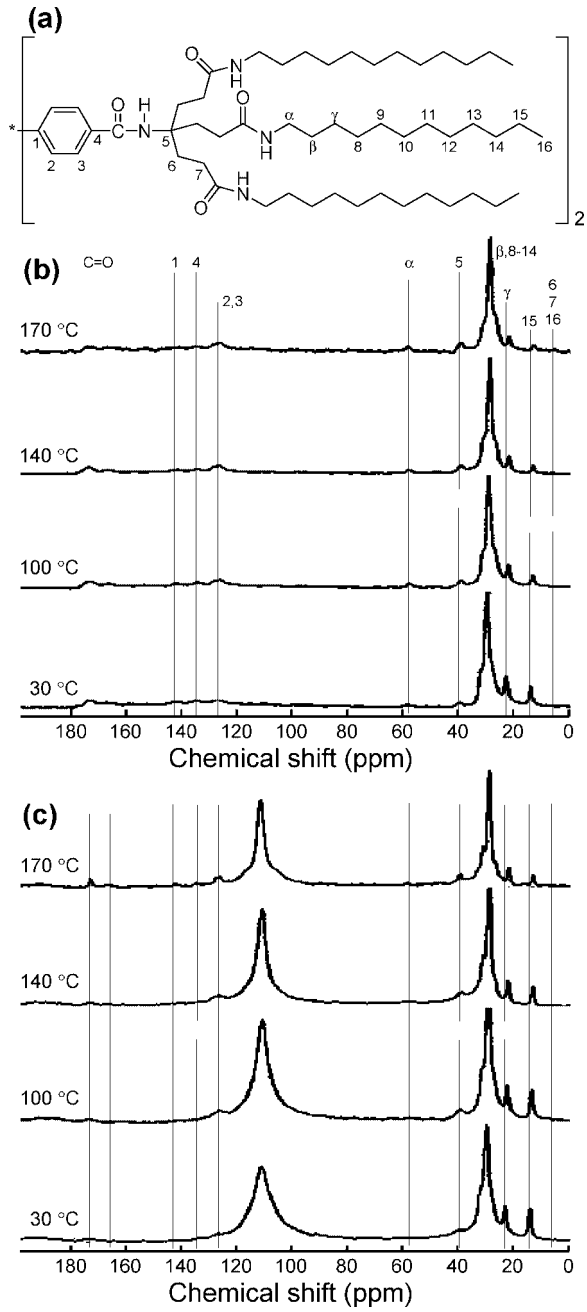


**Figure 5.** Sets of solid-state $^{13}C$ NMR spectra of d-$C_{12}$PhA during heating between 30 and 170 °C: CP/MASS/DD spectra (b) and Bloch decay spectra (c). Chemical shifts of each carbon in d-$C_{12}$PhA are identified in Figure 4a,b.

in the disordered segments of the alkyl chains decreased from 75 to 55%. This result indicates the fact that the methylene carbon atoms in the d-$C_{12}$PhA sample prepared by cooling from the isotropic phase at 2.5 °C/min are more or less in the disordered state at 30 °C and the exothermic transition at 77 °C in DSC thermal diagram (Figure 2a) involves the crystallization of the disordered alkyl chains of d-$C_{12}$PhA. With further increasing temperatures, the area under the chemical shift peak representing the ordered conformations decreases to 40% at 140 °C and to 20% at 170 °C and concurrently the peak area associated with the disordered conformations increased by the same percent. This means that the broad endothermic transition at 145 °C (Figure 2a and 2b) does not much associate with the alkyl chains but the endothermic transition at 153 °C is the melting temperature of the ordered alkyl tails in d-$C_{12}$PhA.

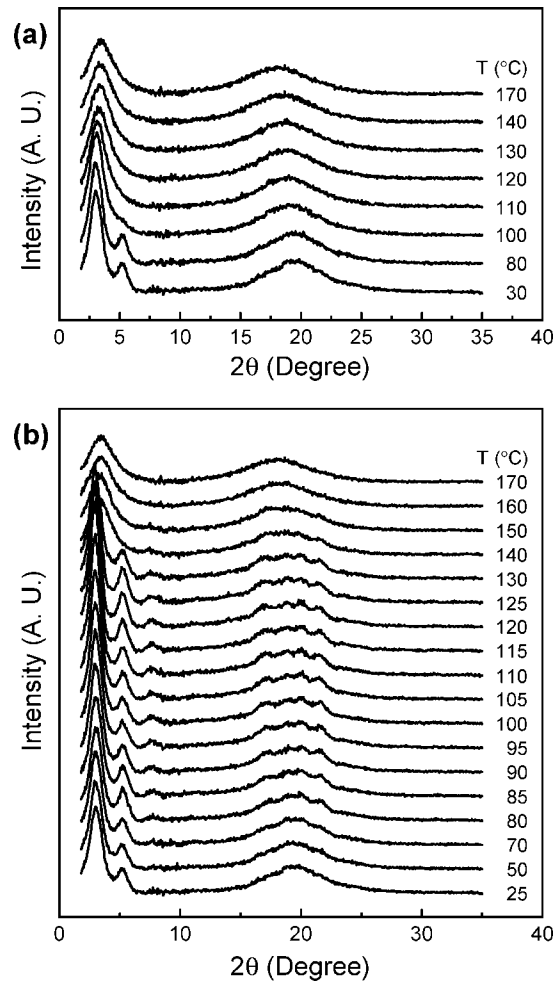


**Figure 6.** Sets of 1D WAXD powder patterns of d-$C_{12}$PhA at a cooling (a) and a subsequent heating (b) rate of 2.5 °C/min at different temperatures.

The FT-IR and solid-state $^{13}C$ NMR results combined with DSC results provide molecular interactions in different phases of d-$C_{12}$PhA on a molecular length scale. In the d-$C_{12}$PhA sample at 30 °C prepared by cooling from the isotropic phase at 2.5 °C/min, all the N−H and C═O groups are associated via H-bonds and the alkyl chains are in the disordered conformations. With increasing the temperature above the exothermic transition at 77 °C, alkyl chains are suddenly in the ordered state, while the H-bonds between N−H and C═O groups are not much changed. Therefore, the broad endothermic transition at 145 °C involves the dissociation of H-bonds of amide groups attached at the end of biphenyls and does not much associate with the alkyl chain conformations. Finally, the endothermic transition at 153 °C is the isotropization process through the dissociation of H-bonds of amide functions in alkyl chains and the disordering of alkyl chain conformations.

**Identifications of Supramolecular Structures of d-$C_{12}$PhA.** Figure 6a and 6b show two sets of 1D WAXD powder patterns of d-$C_{12}$PhA at different temperatures during cooling and subsequent heating at the rate of 2.5 °C/min, respectively. In these figures, structures on two different length scales can be identified. One is on the nanometer scale in the low $2\theta$ angle region between 1.5° and 9°, and the other on the subnanometer scale can be identified between 9° and 30°.

The 1D WAXD powder patterns of d-$C_{12}$PhA in Figure 6a show one-phase transition, and it agrees well with the observation in the DSC cooling diagrams (Figure 2a). At temperatures

above 120 °C, d-$C_{12}$PhA is in the isotropic phase exhibiting only two amorphous halos. One is at $2\theta = 3.42°$ ($d = 2.58$ nm), which may correspond to the average periodicity of electron density fluctuations between aromatic phenyl cores and alkyl chains, and the other is at $2\theta = 18.06°$ ($d = 0.49$ nm), which is attributed to the average distance among the disordered alkyl chains. When the temperature reached below 110 °C, three overlapped low-angle reflections start to emerge and their $2\theta$ angles were identified at $2\theta = 2.98°$, 5.16° and 5.96° ($d = 2.97$, 1.71, and 1.48 nm), respectively, but the intensity of the reflection at $2\theta = 5.96°$ is very weak. The scattering in the high $2\theta$ angle region ($2\theta = 18.06°$) does not change much but gradually moves to $2\theta = 19.47°$ ($d = 0.46$ nm) at 30 °C. Three deconvoluted diffractions in the low $2\theta$ angle region can be assigned to the (10*l*), ($\bar{1}1l$), and (20*l*) diffractions, respectively, based on the triangulation method of building a 2D $a^*b^*$ lattice of the unit cell.[13] The careful construction of the 2D $a^*b^*$ lattice of the unit cell based on the diffractions in the low $2\theta$ angle region provides a 2D hexagonal unit cell with dimensions of $a = 3.41$ nm, $b = 3.41$ nm, and $\gamma = 60°$ via the refinement of the reciprocal lattice, and this phase is abbreviated as the $\Phi_H$ phase. Furthermore, the amorphous halo at $2\theta = 19.47°$ ($d = 0.46$ nm) clearly indicates the fact that alkyl chains are still in the disordered states, which is well matched with the observation on the solid-state $^{13}$C NMR (Figure 5), and the order of aromatic phenyl group phase-on stacking is in the short-range or quasi-long-range order even though the lateral packing of columns are in the long-range order. Here is still an unanswered question: how is a hexagonal columnar phase formed from the linear molecule, d-$C_{12}$PhA? Based on the X-ray diffractions of d-$C_{12}$PhA, a possible formation of a hexagonal columnar phase is proposed, as schematically illustrated in Figure 7. The hydrophilic amide moieties between a rigid hydrophobic biphenyl core and flexible hydrophobic alkyl chains will enhance the phase separation. Together with $\pi-\pi$ stacking interactions between phenyl rings, the intra/intermolecular H-bonds between N−H and C═O functions in the hydrophilic amide moieties are going to stabilize the ordered structure. During the molecular self-assembly process, in order to construct a supramolecular discotic building block, a steric hindrance originating from the relatively big alkyl chains compared with the aromatic core should be accounted for. Considering three main factors described above, a discotic building block can be formed via molecular self-assembly process. As schematically described in Figure 7, three d-$C_{12}$PhA biphenylamides participated and rotated 60° with respect to neighboring ones (ABC stacking) for minimizing the steric hindrances. The self-assembled discotic building block still maintains the intra/intermolecular H-bonds between N−H and C═O functions in the hydrophilic amide moieties, the phase separation, and the $\pi-\pi$ stacking interactions among phenyl rings, which are the main driving forces for the formation of stable ordered phases. Similar to the supermolecular discotic LC mesogens, the self-assembled discotic building blocks will construct columns, and then the columns are laterally close-packed to the hexagonal columnar structure via a self-organization process, as described in Figure 7. It should be noted that flexible hydrophobic alkyl chains at the surface of columns are intercalated with those of close-packed neighboring columns. Based on the unit cell dimensions measured by WAXD and the geometric dimensions of the energy-minimized d-$C_{12}$PhA, the intercalation is ca. 0.62 nm. Note that the alkyl chains are in disordered states at 30 °C, which means alkyl chains of

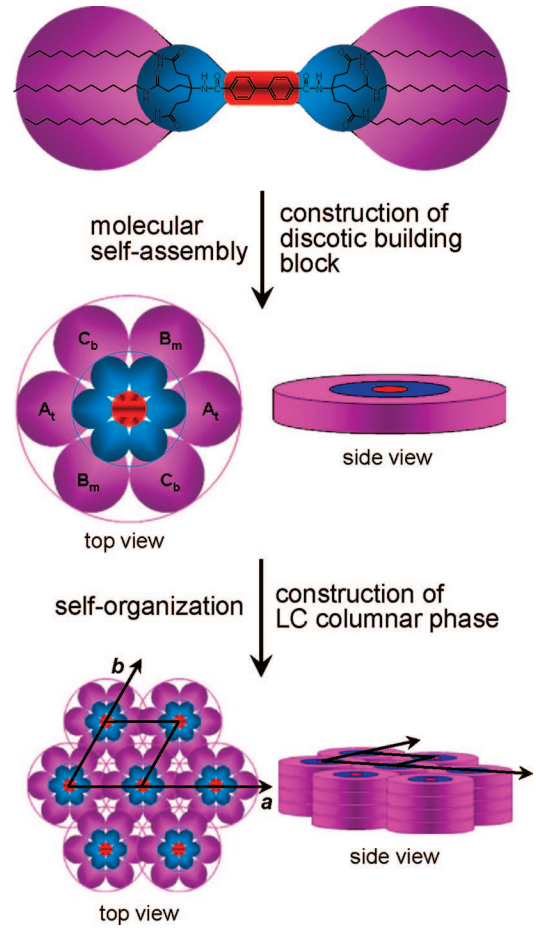


**Figure 7.** Schematic illustrations of the molecular self-assembly and self-organization process for the hexagonal columnar mesophase ($\Phi_H$) of d-$C_{12}$PhA, which is proposed by the analysis of WAXD (Figure 5b).

d-$C_{12}$PhA in one column just fill the empty space of the other column, but do not closely communicate with those in the other columns.

Figures 6b shows a set of 1D WAXD powder patterns of d-$C_{12}$PhA at different temperatures during a subsequent heating rate of 2.5 °C/min after cooling process. As the temperature cross over the exothermic transition at 77 °C, sharp diffractions at $2\theta = 17.2°$, 18.9°, 20.0°, 21.6°, and 23.7° in the high $2\theta$ angle region newly appear together with the diffraction at 7.85°, and there is no significant structural change up to 130 °C. The diffractions in the high $2\theta$ angle region should be associated with the crystallization of alkyl chains, which agrees well with the results of FT-IR (Figures 3 and 4) and solid-state $^{13}$C NMR (Figure 5), and the diffraction at 7.85° should come from the higher order of 2D close-packing of columns. When the temperature is above the onset temperature of endothermic transition at 140 °C, sharp diffractions at $2\theta = 2.97°$ ($d = 2.98$ nm), 5.14° ($d = 1.72$ nm), and 7.85° ($d = 1.13$ nm) suddenly disappear and leave an amorphous halo scattering with a maximum intensity at $2\theta = 3.41°$ ($d = 2.58$ nm). However, the diffractions in the high $2\theta$ angle region are still maintained below the isotropic transition at 153 °C. These WAXD results confirm again that the endothermic transition at 145 °C involves the disordering of columns and the endothermic transition at 153 °C is the isotropization process through the dissociation of H-bonds of amide functions in alkyl chains and the disordering of alkyl chain conformations.

When the packing symmetry of d-$C_{12}$PhA at between 77 and 145 °C is not much different from the 2D hexagonal structure

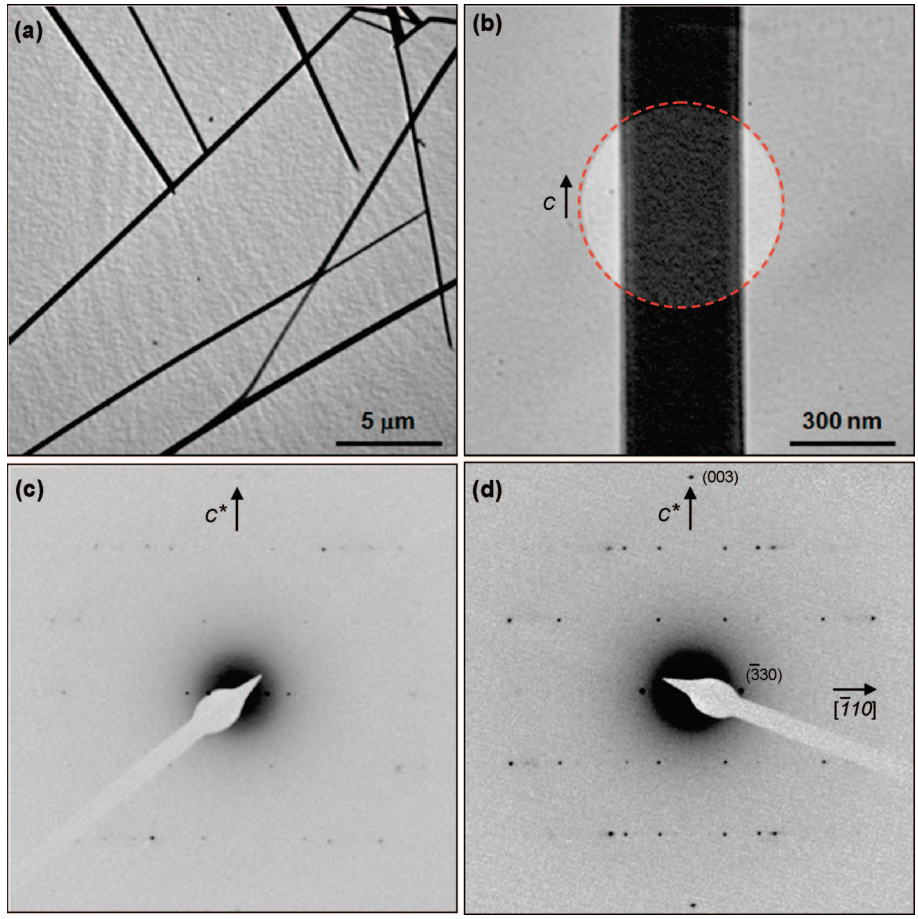


**Figure 8.** Bright-field TEM morphology of the highly ordered hexagonal columnar crystalline phase ($\Phi_{HK}$) of d-$C_{12}$PhA (a). Panel b is the magnified bright-field TEM image and the arrow is pointing along the long axis of the columns (*c* axis). SAED pattern (c) from the circled area of the bright-field TEM morphology in (b). SAED pattern of panel d is obtained by a counterclockwise rotation of the sample in (b) along the *c* axis about 5°.

at 30 °C prepared by slow cooling at 2.5 °C/min, a 2D hexagonal unit cell is constructed with dimensions of $a = 3.44$ nm, $b = 3.44$ nm, $c = 1.13$ nm, $\alpha = \beta = 90°$, and $\gamma = 60°$ via the refinement of the reciprocal lattice,[13] and this phase is abbreviated as the $\Phi_{HK}$ phase. Its calculated crystallographic density is 0.74 g/cm$^3$ based on three d-$C_{12}$PhA molecules per unit cell. The experimentally observed density is 0.74 g/cm$^3$, which fits well with the calculated data.

Even though the 1D WAXD powder experiments at different temperatures combined with the DSC, FT-IR, and solid-state $^{13}$C NMR results can monitor the structural evolutions in d-$C_{12}$PhA compound, 2D WAXD on oriented d-$C_{12}$PhA sample or SAED on single crystals should be conducted to obtain detailed structures and symmetry. Unfortunately, d-$C_{12}$PhA is not oriented under the electrical and magnetic fields as well as under the mechanical flow, which is a required condition prior to beginning 2D WAXD experiments. Therefore, the structural determination and the existence of columns in the $\Phi_{HK}$ phase of d-$C_{12}$PhA can be supported by TEM morphology and SAED pattern experiments. Thin film of d-$C_{12}$PhA samples prepared for TEM via solution casting from a 0.05% (w/v) chloroform solution was heated up to the isotropic temperature and was cooled down to room temperature at 2.5 °C/min, and then was heated up to 100 °C and was waited for 30 min. Figure 8a and 8b show bright-field images of TEM morphology of the highly ordered columnar $\Phi_{HK}$ phase of d-$C_{12}$PhA. As shown in Figure 8a, rods with diameters between 200 and 500 nm were found with the length longer than 500 $\mu$m. The diameters and lengths of rods depend on the cooling and heating rates and annealing time. The existence of columns in the morphology and the packing of discotic building blocks generated by molecular self-assembly and self-organization are confirmed by the SAED pattern as shown in Figure 8c and 8d. SAED taken from the circled area in Figure 8b does not show a high symmetry, as shown in Figure 8c. In order to get a pure [$\bar{1}\bar{1}$0] zone with a high symmetry, the sample in Figure 8b was tilted about 5° counterclockwise around the long axis of the rods and got the SAED represented in Figure 8d. Combined with the results of WAXD (Figure 6b), *c** axis is assigned along the meridian direction and [$\bar{1}\bar{1}$0] direction is along the equator, which are parallel and perpendicular to the long axis of the rod, respectively. On the meridian, only one pair of diffractions is observed at 0.376 nm, which can be the distance of the $\pi-\pi$ stacking interactions between aromatic phenyl rings. This diffraction can be identified to be the (003) and the extinct diffractions at (001) and (002) clearly indicate that the discotic building block is constructed by three d-$C_{12}$PhA biphenylamides rotating 60° with respect to neighboring ones. The ABC stacked discotic building blocks further self-assemble to columns, and these columns are laterally close-packed to hexagonal $\Phi_{HK}$ phase. The next question is that how the columns are arranged in the rods. Based on the diffraction at 0.376 nm on the meridian and the diffraction at 1.72 nm on the equator, the long axis of column should be parallel to the long axis of the rod. However, the diffraction at 1.72 nm determined to be the [$\bar{1}\bar{1}$0] based on the results of 1D WAXD (Figure 6b) should be reassigned to be the [$\bar{3}$30] because

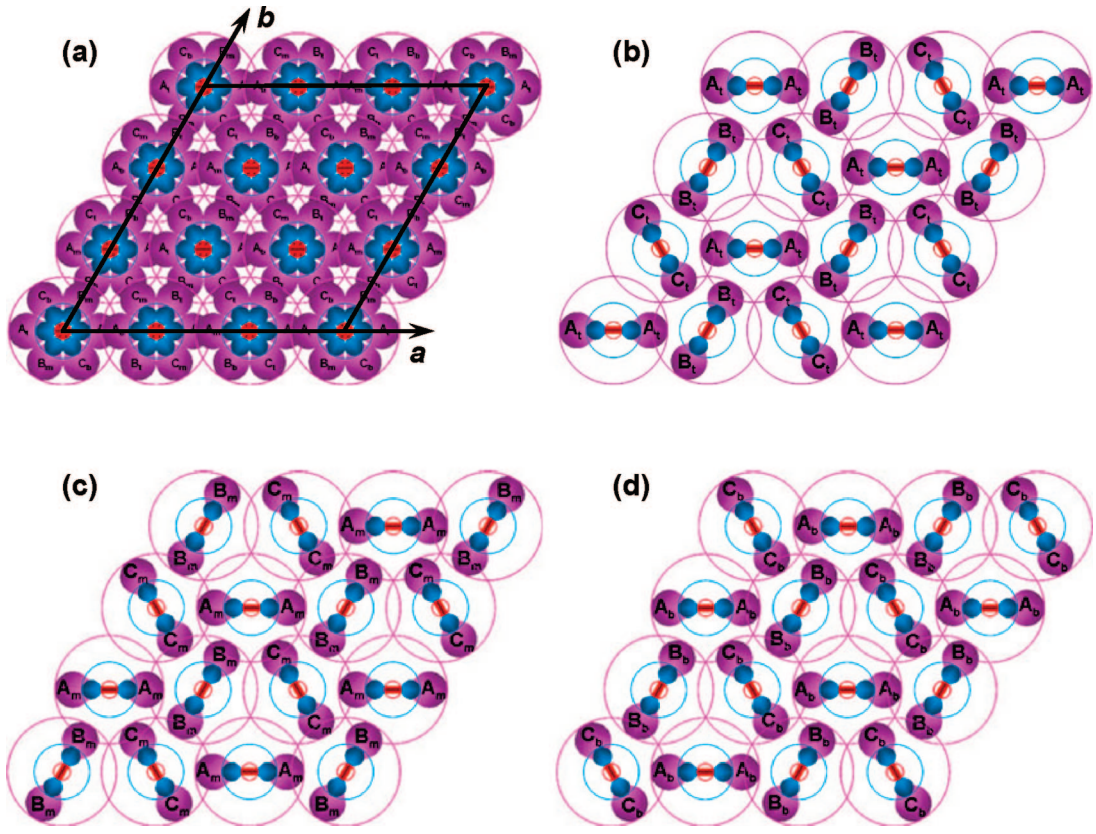


**Figure 9.** Schematic illustrations of the molecular arrangement in the top (b), the middle (c), and the bottom (d) layers of the hexagonal unit cell of $\Phi_{HK}$ phase. When the three layers are combined along the *c* axis, the molecular arrangement in the hexagonal unit cell of $\Phi_{HK}$ phase is constructed, as shown in Figure 8a.

of diffractions in the quadrant regions of SAED (Figure 8d). This means that a hexagonal unit cell of $\Phi_{HK}$ phase should be expanded 3 times along the *a* and *b* axes without changing the packing symmetry, density, and the dimension of *c* axis, as illustrated in Figure 9a. A possible reason can be found from the consideration of the intercalation and recognition of alkyl chains between neighboring columns and the ABC stacking of d-$C_{12}$PhA perpendicular to columnar axis. Based on the unit cell dimensions measured by WAXD and SAED and the geometric dimensions of the energy-minimized d-$C_{12}$PhA, the intercalation is ca. 0.6 nm, and the alkyl chains are in the ordered crystalline state. When a rod is cut and a unit cell is taken out, the unit cell may consist of three planes of molecular packing. They are schematically illustrated in Figure 9b, 9c, and 9d for the top, the middle, and the bottom of the unit cell along the *c* axis, respectively. When three planes are stacked together, the unit cell will be reconstructed, as shown in Figure 9a.

The texture changes in POM can give morphological information on the micrometer length scale, while the bright field image of TEM can give morphological information on the nanometer length scale, and WAXD and SAED provide microscopic structures of the materials.[14] Figure 10a shows the POM micrograph of d-$C_{12}$PhA samples after annealing for 30 min at 100 °C. The POM micrographs of $\Phi_H$ and $\Phi_{HK}$ do not differ much, and do not change until the isotropization temperature. The bright ribbons are the oriented bulk sample. The ribbons are bright because the molecules are in the ordered crystalline phase ($\Phi_{HK}$) and the directions of refractive indexes are not parallel to the directions of the polarizers of the POM. A tint retardation plate (530 nm) was also applied between objective lenses and eyepieces in order to identify the orientation of molecules in the POM textures, as shown in Figure 9b. All

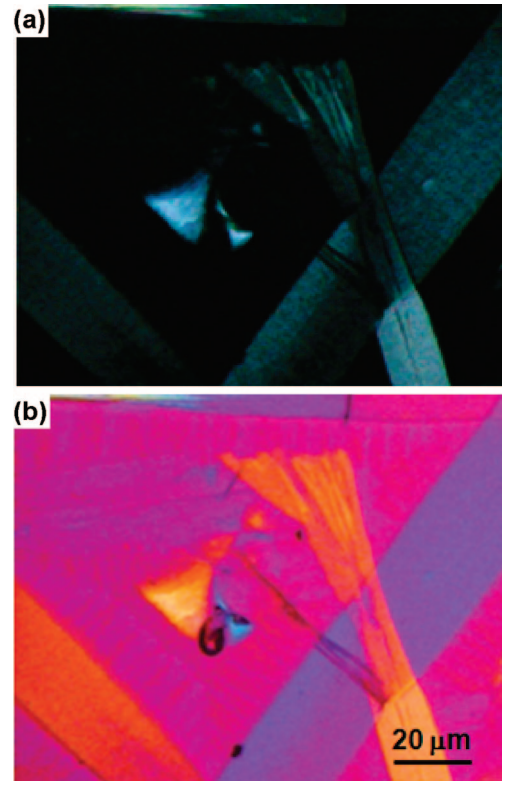


**Figure 10.** POM morphological observations of d-$C_{12}$PhA annealed for 30 min at 100 °C (a) and POM texture with a tint plate between the objective lens and eyepieces (b).

the ribbons going along the direction of left-up to right-down are yellow and all ribbons going along the direction of right-up

to left-down are blue, which means that the refractive index perpendicular to the ribbons ($n_\perp$) is higher than the refractive index parallel to the ribbons ($n_\parallel$). Therefore, the column direction of this supramolecular crystalline columnar phase should align along the long axis of ribbons under POM. This observation is also consistent with the SAED result (Figure 8d).

## Conclusions

Phase behaviors and structures of a newly synthesized symmetrically tapered *N*,*N*′-bis[tris[(2-dodecylaminocarbonyl)-ethyl]methyl]]-4,4′-biphenylamide (d-$C_{12}$PhA, where *n* is the number of carbon atoms in the alkyl chains, $n = 12$) have been investigated based on various experimental techniques. Two ordered phases are identified. The hexagonal columnar ($\Phi_H$) liquid crystalline mesophase is formed during a cooling process, and this $\Phi_H$ phase transforms to a highly ordered hexagonal columnar ($\Phi_{HK}$) crystalline phase during a subsequent heating process. Three major driving forces in the formation of these ordered hexagonal columnar structures participated including the H-bonds between N−H and C═O groups, the phase separation between the aromatic cores and the alkyl chains, and the $\pi-\pi$ stacking interactions between aromatic cores. Based on the results of SAED and WAXD combined with DSC, FT-IR, and solid-state $^{13}$C NMR experiments, we identify that the discotic building block is constructed by three d-$C_{12}$PhA biphenylamides rotating 60° with respect to neighboring ones and the ABC stacked discotic building blocks further self-assemble to columns, and these columns are laterally close-packed to hexagonal columnar phases by a self-organization process. In both ordered hexagonal columnar phases, the alkyl chains are intercalated about 0.6 nm and they are in a disordered state in $\Phi_H$ and in an ordered state in $\Phi_{HK}$. Furthermore, d-$C_{12}$PhA forms nanorods. SAED from the rod allows us to find out the fact that the long axis of column is parallel to the long axis of the nanorods. Phase identifications are further supported by the observation of texture changes in POM, and molecular arrangements inside of the microsize domains were also investigated by introducing a tint plate.

**Acknowledgment.** This work was supported by KRF-2008-314-D00121 and Fundamental R&D Program for Core Technology of Materials funded by the Ministry of Knowledge Economy, Korea.

## References and Notes

(1) (a) Goodby, J. W.; Gray, G. W. *Handbook of Liquid Crystals*; Demus, D., Goodby, J., Gray, G. W., Spiess, H.-W., Vill, V., Eds.; Wiley-VCH: Weinheim, Germany, 1998; Vol. 1, pp 17−23. (b) Demus; D. *Handbook of Liquid Crystals*; Demus, D., Goodby, J., Gray, G. W., Spiess, H.-W., Vill, V., Eds.; Wiley-VCH: Weinheim, Germany, 1998; Vol. 1, pp 133−187. (c) Sage, I. C. *Handbook of Liquid Crystals*; Demus, D., Goodby, J., Gray, G. W., Spiess, H.-W., Vill, V., Eds.; Wiley-VCH: Weinheim, Germany, 1998; Vol. 1, pp 731−762. (d) Crossland, W.; Wilkinson, T. D. *Handbook of Liquid Crystals*; Demus, D., Goodby, J., Gray, G. W., Spiess, H.-W., Vill, V., Eds.; Wiley-VCH: Weinheim, Germany, 1998; Vol. 1, pp 763−822. (e) Cammidge, A. N.; Bushby, R. J. *Handbook of Liquid Crystals*; Demus, D., Goodby, J., Gray, G. W., Spiess, H.-W., Vill, V., Eds.; Wiley-VCH: Weinheim, Germany, 1998; Vol. 2B, pp 693−748. (f) Chandrasekhar, S. *Handbook of Liquid Crystals*; Demus, D., Goodby, J., Gray, G. W., Spiess, H.-W., Vill, V., Eds.; Wiley-VCH: Weinheim, Germany, 1998; Vol. 2B, pp 749−780. (g) Hoffmann, S. *Handbook of Liquid Crystals*; Demus, D., Goodby, J., Gray, G. W., Spiess, H.-W., Vill, V., Eds.; Wiley-VCH: Weinheim, Germany, 1998; Vol. 3, pp 393−452.

(2) (a) Tschierske, C. *J. Mater. Chem.* **1998**, *8*, 1485. (b) Ichimura, K. *Chem. Rev.* **2000**, *100*, 1847. (c) Shan, R. R.; Abbott, N. L. *J. Phys. Chem. B* **2001**, *105*, 4936. (d) Araos, M. U.; Warr, G. G. *J. Phys. Chem. B* **2005**, *109*, 14275. (e) Saez, I. M.; Goodby, J. W. *J. Mater. Chem.* **2005**, *15*, 26. (f) Cook, A. G.; Baumeister, U.; Tschierske, C. *J. Mater. Chem.* **2005**, *15*, 1708. (g) Yablon, D. G.; Wintgens, D.; Flynn, G. W. *J. Phys. Chem. B* **2002**, *106*, 5470. (h) Wang, P.; Moorefield, C. N.; Jeong, K.-U.; Hwang, S.-H.; Li, S.; Cheng, S. Z. D.; Newkome, G. R. *Adv. Mater.* **2008**, *20*, 1381. (i) Sui, G.; Orbulescu, J.; Mabrouki, M.; Micic, M.; Leblanc, R. M.; Liu, S. G.; Cormier, R. A.; Gregg, B. A. *J. Phys. Chem. B* **2002**, *106*, 9335. (j) Rodriguez-Abreu, C.; Izawa, T.; Aramaki, K.; Lopez-Quintela, A.; Sakamoto, K.; Kunieda, H. *J. Phys. Chem. B* **2004**, *108*, 20083. (k) Park, H. S.; Kang, S. W.; Tortora, L.; Nastishin, Y.; Finotello, D.; Kumar, S.; Lavrentovich, O. D. *J. Phys. Chem. B* **2008**, *112*, 16307.

(3) (a) Jeong, K.-U.; Jin, S.; Ge, J. J.; Knapp, B. S.; Graham, M. J.; Ruan, J.; Guo, M.; Xing, H.; Harris, F. W.; Cheng, S. Z. D. *Chem. Mater.* **2005**, *17*, 2852. (b) Jeong, K.-U.; Knapp, B. S.; Ge, J. J.; Jin, S.; Graham, M. J.; Xiong, H.; Harris, F. W.; Cheng, S. Z. D. *Macromolecules* **2005**, *38*, 8333. (c) Jeong, K.-U.; Knapp, B. S.; Ge, J. J.; Jin, S.; Graham, M. J.; Harris, F. W.; Cheng, S. Z. D. *Chem. Mater.* **2006**, *18*, 680. (d) Jeong, K.-U.; Knapp, B. S.; Ge, J. J.; Graham, M. J.; Tu, Y.; Leng, S.; Xiong, H.; Harris, F. W.; Cheng, S. Z. D. *Polymer* **2006**, *47*, 3351. (e) Jeong, K.-U.; Yang, D. K.; Graham, M. J.; Tu, Y.; Kuo, S. W.; Knapp, B. S.; Harris, F. W.; Cheng, S. Z. D. *Adv. Mater.* **2006**, *18*, 3229. (f) Jeong, K.-U.; Jing, A. J.; Monsdorf, B.; Graham, M. J.; Harris, F. W.; Cheng, S. Z. D. *Chem. Mater.* **2007**, *19*, 2921. (g) Jeong, K.-U.; Jing, A. J.; Monsdorf, B.; Graham, M. J.; Harris, F. W.; Cheng, S. Z. D. *J. Phys. Chem. B* **2007**, *110*, 767. (h) Jeong, S. J.; Sureshkumar, P.; Jeong, K.-U.; Lee, S. H.; Jeong, S. H.; Lee, Y. E.; Lu, R.; Wu, S. T. *Opt. Express* **2007**, *15*, 11698. (i) Wang, L.; Jeong, K.-U.; Lee, M.-H. *J. Mater. Chem.* **2008**, *18*, 2657. (j) Yang, D.-K.; Jeong, K.-U.; Cheng, S. Z. D. *J. Phys. Chem. B* **2008**, *112*, 1358.

(4) (a) Vaughan, G. B. M.; Heiney, P. A.; McCauley III, Jr J. P.; Smith, A. B. *Phys. Rev B* **1992**, *46*, 2787. (b) Boden, N.; Bushby, R. J.; Clements, J. *J. Chem. Phys.* **1993**, *98*, 5920. (c) Arikainen, E. O.; Boden, N.; Bushby, R. J.; Clements, J.; Movaghar, B.; Wood, A. *J. Mater. Chem.* **1995**, *5*, 2161. (d) Matsui, T.; Nagata, T.; Ozaki, M.; Fujii, A.; Onoda, M.; Teraguchi, M.; Masuda, T.; Yoshino, K. *Synth. Met.* **2001**, *119*, 599.

(5) (a) Adam, D.; Closs, F.; Frey, T.; Funhoff, D.; Haarer, D.; Ringsdorf, H.; Schuhmacher, P.; Siemensmeyer, K. *Phys. Rev. Lett.* **1993**, *70*, 457. (b) Adam, D.; Schuhmacher, P.; Simmerer, J.; Haussling, L.; Siemensmeyer, K.; Etzbach, K. H.; Ringsdorf, H.; Haarer, D. *Nature (London)* **1994**, *371*, 141. (c) Bengs, H.; Closs, F.; Frey, T.; Funhoff, D.; Ringsdorf, H.; Siemensmeyer, K. *Liq. Cryst.* **1993**, *15*, 565. (d) Closs, F.; Siemensmeyer, K.; Frey, T.; Funho, D. *Liq. Cryst.* **1993**, *14*, 629. (e) Boden, N.; Bushby, R. J.; Clements, J.; Movaghar, B.; Donovan, K. J.; Kreouzis, T. *Phys. Rev. B* **1995**, *52*, 13274. (f) Simmerer, J.; Glusen, B.; Paulus, W.; Kettner, A.; Schuhmacher, P.; Adam, D.; Etzbach, K.; Siemensmeyer, K.; Wendorff, J. H.; Ringsdorf, H.; Haarer, D. *Adv. Mater.* **1996**, *8*, 815.

(6) (a) Bock, H.; Helfrich, W. *Liq. Cryst.* **1992**, *12*, 697. (b) Bock, H.; Helfrich, W. *Liq. Cryst.* **1995**, *18*, 387.

(7) (a) Hoger, S.; Enkelmann, V.; Bonrad, K.; Tschierske, C. *Angew. Chem. Int. Ed.* **2000**, *39*, 2268. (b) Phillips, K. E. S.; Katz, T. J.; Jockusch, S.; Lovinger, A. J.; Turro, N. J. *J. Am. Chem. Soc.* **2001**, *123*, 11899. (c) Kanie, K.; Nishii, M.; Yasuda, T.; Taki, T.; Ujiie, S.; Kato, T. *J. Mater. Chem.* **2001**, *11*, 2875. (d) Rais, K.; Daoud, M.; Gharbia, M.; Gharbi, A.; Nguyen, H. T. *ChemPhysChem* **2001**, *2*, 45. (e) Kishikawa, K.; Furusawa, S.; Yamaki, T.; Kohmoto, S.; Yamamoto, M.; Yamaguchi, K. *J. Am. Chem. Soc.* **2002**, *124*, 1597. (f) Jung, H.-T.; Kim, S. O.; Ko, Y. K.; Yoon, D. K.; Hudson, S. D.; Percec, V.; Holerca, M. N.; Cho, W.-D.; Mosier, P. E. *Macromolecules* **2002**, *35*, 3717.

(8) (a) Hunter, C. A.; Sanders, J. K. M. *J. Am. Chem. Soc.* **1990**, *112*, 5525. (b) Lehn, J. M. *Science* **2002**, *295*, 2400. (c) Messmore, B. W.; Sukerkar, P. A.; Stupp, S. I. *J. Am. Chem. Soc.* **2005**, *127*, 7992. (d) Yang, W.; Chai, X.; Chi, L.; Liu, X.; Cao, Y.; Lu, R.; Jiang, Y.; Tang Fuchs, X. H.; Li, T. *Chem.—Eur. J.* **1999**, *5*, 1144. (e) Hirschberg, J. H.; Brunsveld, L.; Ramzi, A.; Vekemans, J. A.; Sijbesma, R. P.; Meijer, E. W. *Nature (London)* **2000**, *407*, 167. (f) Kato, T.; Mizoshita, N.; Kanie, K. *Macromol. Rapid Commun.* **2001**, *22*, 797. (g) Kato, T. *Science* **2002**, *295*, 2414. (h) Reinhoudt, D. N.; Drego-Calama, M. *Science* **2002**, *295*, 2403. (i) Keinan, S.; Ratner, M. A.; Mark, T. J. *Chem. Mater.* **2004**, *16*, 1848. (j) Jin, S.; Ma, Y.; Zimmerman, S. C.; Cheng, S. Z. D. *Chem. Mater.* **2004**, *16*, 2975.

(9) (a) Ungar, G.; Abramic, D.; Percec, V.; Heck, J. A. *Liq. Cryst.* **1996**, *21*, 73. (b) Xue, C.; Jin, S.; Weng, X.; Ge, J. J.; Shen, Z.; Shen, H.; Graham, M. J.; Jeong, K.-U.; Huang, H.; Zhang, D.; Guo, M.; Harris, F. W.; Cheng, S. Z. D. *Chem. Mater.* **2004**, *16*, 1014. (c) Shen, H.; Jeong, K.-U.; Xiong, H.; Graham, M. J.; Leng, S.; Zheng, J. X.; Huang, H.; Guo, M.; Harris, F. W.; Cheng, S. Z. D. *Soft Matter* **2006**, *2*, 232. (d) Shen, H.; Jeong, K.-U.; Graham, M. J.; Leng, S.; Huang, H.; Lotz, B.; Hou, H.; Harris, F. W.; Cheng, S. Z. D. *J. Macromol. Sci., Part B: Phys.* **2006**, *45*, 215.

(10) (a) Klausner, Y. S.; Bodansky, M. *Synthesis* **1972**, 453. (b) Newkome, G. R.; Moorefield, C. N.; Baker, G. R. *Aldrichim. Acta* **1992**, *25*, 31. (c) Newkome, G. R.; Weis, C. D. *Org. Prep. Proced. Int.* **1996**, *28*, 242. (d) Han, S.-Y.; Kim, Y.-A. *Tetrahedron* **2004**, *60*, 2447.

(11) (a) Pavia, D. L.; Lampman, G. M.; Kriz, G. S. *Introduction to Spectroscopy*, 2nd ed.; Harcourt Brace College Publishers: Austin, TX, 1996.;(b) MacPhail, R. A.; Strauss, H. L.; Snyder, R. G.; Elliger, C. A. *J. Phys. Chem.* **1984**, *88*, 334. (c) Venkataraman, N. V.; Vasudevan, S. *J. Phys. Chem. B* **2001**, *105*, 1805. (d) Noda, I.; Ozaki, Y. *Two-Dimensional Correlation Spectroscopy*; John Wiley & Sons: New York, 2004.

(12) (a) Bovey, F. A.; Mirau, P. A. *NMR of Polymers*; Academic Press: San Diego, CA, 1996. (b) Cheng, J.; Jin, Y.; Wunderlich, B.; Cheng, S. Z. D.; Yandrasits, M. A.; Zhang, A.; Percec, V. *Macromolecules* **1992**, *25*, 5991. (c) Cheng, J.; Yoon, Y.; Ho, R.-M.; Leland, M.; Guo, M.; Cheng, S. Z. D.; Chu, P.; Percec, V. *Macromolecules* **1997**, *30*, 4688. (d) McElheny, D.; Grinshtein, J.; Frydman, V.; Frydman, L. *Macromolecules* **2002**, *35*, 3544. (e) Ishida, H.; Horii, F. *Macromolecules* **2002**, *35*, 5550.

(13) (a) Eashoo, M.; Wu, Z.; Zhang, A.; Shen, D.; Tse, C.; Harris, F. W.; Cheng, S. Z. D.; Gardner, K. H.; Hsiao, B. S. *Macromol. Chem. Phys.* **1994**, *195*, 2207. (b) Seddon, J. M. *Handbook of Liquid Crystals*; Demus, D., Goodby, J., Gray, G. W., Spiess, H.-W., Vill, V., Eds.; Wiley-VCH: Weinheim, Germany, 1998; Vol. 1, pp 635−679. (c) Ye, C.; Xu, G.; Yu, Z. Q.; Lam, J. W. Y.; Jang, J. H.; Peng, H. L.; Tu, Y.; Liu, Z. F.; Jeong, K.-U.; Cheng, S. Z. D.; Chen, E.-Q.; Tang, B. Z. *J. Am. Chem. Soc.* **2005**, *127*, 7668. (d) Ruan, J.-J.; Ge, J. J.; Jin, S.; Jeong, K.-U.; Graham, M. J.; Zhang, D.; Harris, F. W.; Lotz, B.; Cheng, S. Z. D. *Polymer* **2006**, *47*, 4182. (e) Jin, S.; Jeong, K.-U.; Li, C. Y.; Bai, F.; Harris, F. W.; Cheng, S. Z. D.; Lotz, B. *Macromolecules* **2007**, *40*, 5450.

(14) Dierking, I. *Textures of Liquid Crystals*; Wiley-VCH: Weinheim, Germany, 2003.

JP900666C